


RESEARCH

Open Access



# GPR56 function as a key repressor in hepatocyte pyroptosis and the pathogenesis of liver fibrosis

Zhemini Shi<sup>1†</sup>, Qi Liu<sup>1†</sup>, Mengxia Zhang<sup>1†</sup>, Xiaoxiao Du<sup>1†</sup>, Yifan He<sup>1</sup>, Lina Zheng<sup>1</sup>, Wei Hong<sup>1\*</sup>, Tao Han<sup>2\*</sup> and Kun Zhang<sup>1\*</sup> 

## Abstract

**Background** Given the rising prevalence of liver fibrosis, there is an urgent need to improve the effective diagnostic methods and treatment of liver fibrosis. Although GPCRs are involved in various physiological and pathological processes, however, the hepatic functions of GPR56 have rarely been explored. This study aims to investigate the role and underlying mechanisms of GPR56 in liver fibrosis.

**Methods** The expression of GPR56 in carbon tetrachloride (CCl<sub>4</sub>) and bile duct ligation (BDL) induced mouse liver fibrosis, as well as human fibrotic liver tissues, was assessed by western blot, qRT-PCR and immunohistochemistry. Then, WGCNA combined with GO enrichment analysis were employed to predict the functions of GPR56. Additionally, Gain- and loss-of-function models (in vitro and in vivo) were established to explore GPR56's function and the signaling pathways involved in liver fibrosis and hepatocyte pyroptosis.

**Results** GPR56 was upregulated in both human and mouse fibrotic liver tissues, as well as hepatocytes from CCl<sub>4</sub>-induced liver fibrosis mice. ROC analysis showed high diagnostic accuracy for cirrhosis (AUC = 0.895, 95% CI: 0.783–1.000). Moreover, WGCNA and GO enrichment analysis speculated that GPR56 was involved in the inflammatory response and extracellular matrix (ECM) synthesis. In vivo assays revealed that hepatocyte-specific overexpression of GPR56 attenuated, while knockdown of GPR56 exacerbated NLRP3 inflammasome-mediated pyroptosis and liver fibrosis. In vitro experiments confirmed that GPR56 inhibited hepatocyte pyroptosis, leading to the inactivation of hepatic stellate cells (HSC). Mechanistic experiments further revealed that GPR56 attenuated hepatocyte pyroptosis via inhibiting the activation of NF-κB pathway.

<sup>†</sup>Zhemini Shi, Qi Liu, Mengxia Zhang and Xiaoxiao Du contributed equally to this work.

\*Correspondence:

Wei Hong

hongwei@tmu.edu.cn

Tao Han

hantaomd@126.com

Kun Zhang

zhangkun@tmu.edu.cn

Full list of author information is available at the end of the article



© The Author(s) 2025. **Open Access** This article is licensed under a Creative Commons Attribution-NonCommercial-NoDerivatives 4.0 International License, which permits any non-commercial use, sharing, distribution and reproduction in any medium or format, as long as you give appropriate credit to the original author(s) and the source, provide a link to the Creative Commons licence, and indicate if you modified the licensed material. You do not have permission under this licence to share adapted material derived from this article or parts of it. The images or other third party material in this article are included in the article's Creative Commons licence, unless indicated otherwise in a credit line to the material. If material is not included in the article's Creative Commons licence and your intended use is not permitted by statutory regulation or exceeds the permitted use, you will need to obtain permission directly from the copyright holder. To view a copy of this licence, visit <http://creativecommons.org/licenses/by-nc-nd/4.0/>.

**Conclusions** Our study identifies GPR56 as a suppressor of hepatocyte pyroptosis and liver fibrosis, underscoring its potential as a therapeutic and diagnostic target.

**Keywords** Liver fibrosis, GPCR, Hepatocytes, Pyroptosis, Hepatic stellate cells, NF- $\kappa$ B

## Background

Liver fibrosis represents a pathological response to chronic liver injury, characterized by the aberrant deposition of connective tissue within the liver. This leads to structural disruption and subsequent functional impairment of hepatic tissue [1–5]. Early-stage liver fibrosis can be managed or potentially reversed with prompt and efficacious intervention. Conversely, delayed or inadequate treatment can escalate to cirrhosis or hepatocellular carcinoma. Although current therapeutic approaches including chemotherapy, surgical resection, liver transplantation, and emerging targeted and immunotherapies have improved outcomes for patients with cancer or liver failure [6–10], the global burden of chronic liver diseases remains substantial. This is largely due to the complex etiology of liver pathologies, such as viral hepatitis, alcoholic liver disease, and non-alcoholic fatty liver disease, which contribute to rising incidence rates worldwide [1, 2]. As a pivotal intermediate stage in the progression of chronic liver diseases towards cirrhosis and cancer, liver fibrosis poses a significant threat to global health. Therefore, elucidating the pathogenic mechanisms of liver fibrosis and developing novel diagnostic and therapeutic strategies are of paramount clinical importance for improving patient prognosis [1, 2, 11].

The G protein coupled receptor (GPCR) family is enormous and more than 800 GPCRs have been classified in the human genome. Notably, approximately 30% of commercially available drugs target GPCRs [12]. Structurally, GPCRs are characterized by their seven-transmembrane helices. Alterations in expression or conformational changes of GPCRs can significantly alter intracellular signaling pathways, thereby influencing a myriad of physiological and pathological processes [13–16]. Therefore, the study of the physiological processes in which GPCRs may be involved and their specific ligands is of great importance for the treatment of diseases.

GPR56 (ADGRG1) belongs to the adhesion GPCRs (aGPCRs) subgroup located on the human chromosome 16q21 and consists of 14 exons [17]. It was the first aGPCR with identified ligands, including CD9/CD81, transglutaminase 2 (TG2) and type III collagen [18–20]. GPR56 exhibits a broad distribution across human organs, including the brain, thyroid, kidney, skeletal muscle and hematopoietic system [21]. The most well-established function of GPR56 is its critical role in cerebral cortex development [22]. Mutations in GPR56 have been reported to trigger a rare familial genetic disorder of the cerebral cortex, namely bilateral

frontoparietal polymicrogyria (BFPP), further supporting the integral role of GPR56 in cerebral cortex development [23]. Additionally, GPR56 also plays a role in regulating the proliferation of oligodendrocyte precursor cells (OPCs) and myelin repair in neurons within the central nervous system. One study found that GPR56 is expressed in two animal models of myelin repair and promotes the proliferation of OPCs during development [24]. Furthermore, GPR56 has been implicated in exerting antidepressant-like effects, and chronic stress in mice leads to a significant reduction in GPR56 expression in the blood, prefrontal cortex, and dorsal hippocampal regions. This downregulation correlates with the manifestation of depression-like behaviors, which are reversible upon treatment with antidepressants [25]. Moreover, GPR56 is involved in the development of several tumors. GPR56 has been shown to enhance colorectal cancer cells (CRC) metastasis by activating the PI3K/AKT signaling pathway, thereby promoting the EMT process [26]. In human melanoma cells, activation of GPR56 induces interleukin-6 (IL-6) secretion and promotes cell migration and invasion through the G $\alpha$ 12/13-Rho pathway [27]. However, the role of GPR56 in hepatic function has rarely been reported. Therefore, in this study, we aim to elucidate the biological function of GPR56 in liver fibrosis through bioinformatics and multifaceted biological experiments, with the objective of assessing its potential of GPR56 as a diagnostic and therapeutic target for liver fibrosis.

## Materials and methods

### Data source and analysis

The GEO database was searched for data sets related to liver fibrosis, and the data set from the rat BDL model GSE174099 and the data set from human cirrhosis GSE25097 were identified (Table S1). Subsequently, differential gene expression analysis was performed using GEO2R, focusing on genes with  $P_{adj} < 0.05$  and  $|\log_2FC| \geq 1$ . The resulting datasets were then intersected with a list of 33 aGPCRs, and the aGPCRs with significantly differential expression in liver fibrosis were identified.

### Cell culture

HEK293T and AAV293 cells were cultured in Dulbecco's modified Eagle's medium (DMEM, Invitrogen, Camarillo, CA) supplemented with 10% fetal bovine serum (FBS, Gibco, Gaithersburg, MD, USA), penicillin (100U/ml) and streptomycin (100  $\mu$ g/ml). All cells were cultured at 37 °C with 5% CO<sub>2</sub>.

### In vivo study of animals

The animal protocols were approved by the Animal Care and Use Committee of Tianjin Medical University. Methods were carried out in accordance with the approved guidelines and the code of ethical approval is TMUaMEC2023022. All Balb/c and C57BL/6J mice aged 6 weeks and with the body weight of approximately 21 g were obtained from Beijing HFK bioscience (Beijing, China). The mice were then fed normally for one week after all mice were injected with 100  $\mu$ l of adeno-associated virus through the tail vein. For hepatocyte-specific overexpression experiments, all Balb/c mice were randomly divided into 4 groups, AAV8-TBG group (AAV8-TBG-Ctrl,  $n=6$ ), AAV8-TBG + CCl<sub>4</sub> group (AAV8-TBG-Ctrl + CCl<sub>4</sub>,  $n=8$ ), AAV8-TBG-GPR56 group (AAV8-TBG-GPR56,  $n=6$ ) and AAV8-TBG-GPR56 + CCl<sub>4</sub> group (AAV8-TBG-GPR56 + CCl<sub>4</sub>,  $n=8$ ), respectively. One week after AAV8 injection, mice in the CCl<sub>4</sub> (Sigma-Aldrich, St. Louis, MO, USA) group were started to be injected intraperitoneally with 5% CCl<sub>4</sub> (v/v) dissolved in olive oil (0.3 ml/kg body weight) three times a week for 6 weeks, and mice in the control group were weighed and injected intraperitoneally with an equal volume of olive oil. Similarly, all C57BL/6J mice were also divided into 4 groups, AAV8-TBG group (AAV8-TBG-Ctrl,  $n=6$ ), AAV8-TBG + BDL group (AAV8-TBG-Ctrl + BDL group,  $n=10$ ), AAV8-TBG-GPR56 group (AAV8-TBG-GPR56,  $n=6$ ) and AAV8-TBG-GPR56 + BDL group (AAV8-TBG-GPR56 + BDL,  $n=10$ ). One week after AAV8 injection, mice in the BDL group underwent BDL surgery, and mice were executed 21 days after surgery. Regarding the knockdown experiments, Balb/c mice were randomly divided into 4 groups, AAV8-NC group (AAV8-NC,  $n=6$ ), AAV8-NC + CCl<sub>4</sub> group (AAV8-NC + CCl<sub>4</sub>,  $n=8$ ), AAV8-GPR56-shRNA group (GPR56-shRNA,  $n=6$ ) and AAV8-GPR56-shRNA + CCl<sub>4</sub> group (GPR56-shRNA + CCl<sub>4</sub>,  $n=8$ ), respectively. One week after AAV8 injection, mice in the CCl<sub>4</sub> (Sigma-Aldrich, St. Louis, MO, USA) group were started to be injected intraperitoneally with 5% CCl<sub>4</sub> (v/v) dissolved in olive oil (0.3 ml/kg body weight) three times a week for 6 weeks, and mice in the control group were weighed and injected intraperitoneally with an equal volume of olive oil. Finally, the mice were anesthetized with 60–100  $\mu$ l of 2% pentobarbital sodium, and blood was collected via enucleation of the eyeball. The supernatant was obtained by centrifugation and stored at  $-20^{\circ}\text{C}$  for subsequent experiments. The animals were sacrificed by cervical dislocation after blood collection. Next, the abdominal cavity was opened, and the liver was grasped with tweezers. The surrounding connective tissue was dissected with scissors, and the liver was excised. The liver was then cut into small pieces, rapidly frozen in liquid nitrogen, and stored at  $-80^{\circ}\text{C}$  for long-term use in subsequent

experiments. After the animal experiments were completed, the mice carcasses were wrapped and sealed in special biohazard bags, then placed in the freezer designated by the Laboratory Animal Center for centralized freezing storage and subsequent disposal.

### Histology and immunohistochemistry (IHC)

Liver tissues were fixed in a 10% neutral buffered formaldehyde solution for 48 h. Subsequently, the tissues were dehydrated in gradient ethanol solution and transparent in xylene solution. The processed tissues were then embedded in paraffin, and 5-micrometer-thick Sect. (5  $\mu$ m) were prepared. These sections were stained with Hematoxylin and Eosin (H&E), Sirius Red (Solarbio), Masson's trichrome (Solarbio), and Terminal deoxynucleotidyl transferase dUTP nick-end labeling (TUNEL) (Roche), respectively. For IHC analysis, slides were subjected to antigen retrieval in antigen repair solution at  $108^{\circ}\text{C}$  for 5 min, followed by a 15-minute incubation in 3% hydrogen peroxide (H<sub>2</sub>O<sub>2</sub>) to block endogenous peroxidase activity, protected from light. After washing with 1 $\times$  phosphate-buffered saline (PBS) for 15 min at room temperature, the sections were incubated with goat serum (50–100  $\mu$ l) for 30 min at  $37^{\circ}\text{C}$  to reduce non-specific binding. Primary antibodies against  $\alpha$ -SMA (1:50, rabbit polyclonal, Abcam, ab5694) and GPR56 (1:50, mouse monoclonal, Sigma, MABN310) were incubated at  $4^{\circ}\text{C}$  for 16 h, while negative controls were treated with an equal volume of 1 $\times$ PBS. After the primary antibody was recovered, 1 $\times$ PBS was washed at room temperature for 15 min and the secondary antibody was added and incubated for 2 h at room temperature avoiding light, then the staining was terminated with distilled water using DAB staining and observing the positive specimens under the microscope when brown areas appeared and the background color was light. Finally, the sections were re-stained with hematoxylin for 2 min and then gradient dehydrated with ethanol solution and sealed, with microscopic photographs taken of the sections and the degree of tissue fibrosis was assessed.

### qRT-PCR

Tissue or cellular RNA was extracted using Trizol (Takara, China) and reverse transcribed into cDNA using PrimeScript RT Reagent Kit (Takara, China) according to the manufacturer's instructions, and further qRT-PCR was used to identify the expression of genes in tissues or cells. The specific primer sequences are shown in the Table S2.

### Western blot

Tissue or cell RIPA lysates (including 1% PMSF and 1% phosphatase inhibitor) were lysed on ice for 30 min, then the supernatant was collected after centrifugation

at 4 °C, 14,000 rpm for 30 min, and the protein concentration was determined using the BCA kit for sample preparation. Next, we separated the proteins by SDS-PAGE gel electrophoresis, and transferred them to the PVDF membrane, which was blocked with 5% skim milk for 1 h and then added specific primary antibody overnight at 4 °C. The next day, the corresponding secondary antibody (1:10,000) was added and incubated at room temperature for 1 h. Finally, the protein content was detected by developing with an ECL luminescent solution. Primary antibodies included TIMP1 (1:1000, mouse monoclonal, Santa Cruz, sc-21734), MMP2 (1:2000, rabbit monoclonal, Abcam, ab92536),  $\alpha$ -SMA (1:1000, rabbit polyclonal, Abcam, ab5694), GPR56 (1:1000, mouse monoclonal, Sigma, MABN310), NLRP3 (1:1000, rabbit monoclonal, CST, 15101), Caspase1 (1:1000, rabbit monoclonal, Abcam, ab34710), GSDMD (1: 1000, rabbit monoclonal, Abcam, ab209845), COL1 $\alpha$ 1 (1:1000, rabbit polyclonal, Abcam, ab34710), IKK (1:1000, rabbit monoclonal, Abcam, ab178870), phos-IKK (1:1000, rabbit monoclonal, CST, 2697), I $\kappa$ B $\alpha$  (1:1000, mouse monoclonal, CST, 4814), phos-I $\kappa$ B $\alpha$  (1:1000, mouse monoclonal, CST, 9246), p65 (1:1000, mouse monoclonal, Santa Cruz, sc-8008), phos-p65 (1:1000, rabbit monoclonal, CST, 3033), GAPDH as internal reference.

#### Isolation of primary HC and HSC

Primary HSC and hepatocyte (HC) were isolated by collagenase perfusion digestion and density gradient centrifugation as previously reported [28–32]. Enzymes required for cell isolation include collagenase type IV (Sigma-Aldrich, St. Louis, MO, USA), proteinase E (Roche, Mannheim, Germany), and DNase I (Roche). 8-week-old male Balb/c mice were used to isolate HC. The liver was first exposed and perfused sequentially with 30 ml of SCI solution and 30 ml of 0.05% collagenase IV solution. Then, after centrifugation at 4 °C, 50 g for 4 min, the supernatant was discarded and the precipitate was retained and repeated 3 times, the last time the precipitate was resuspended and spread on collagen-coated culture plates. The HSC isolation using 40-week male Balb/c mice. The liver was first exposed and perfused sequentially with 30 ml of SCI solution, 30 ml of 0.05% proteinase E solution and 30 ml of 0.05% collagenase IV solution. Then, the supernatant was collected by centrifugation at 4 °C, 50 g for 4 min. Next, centrifuge at 550 g for 8 min at 4°C, keep the precipitate, add 18% Nycodenz solution (Sigma-Aldrich) and mix the precipitate, then slowly add 12% and 8% Nycodenz solution and DMEM, centrifuge at 1450 g for 30 min at 4°C, with no brake power. The DMEM and 8% gradient centrifugation solution was slowly aspirated using a disposable dropper and transferred to a new centrifuge tube, the mixture was resuspended and centrifuged at 4 °C, 600 g for 6 min, and

the precipitate was HSC. Finally, complete cell medium was added and spread the plate. Both primary HC and HSC were cultured with DMEM medium, 10% FBS and 1% penicillin-streptomycin antibiotics. All cells were cultured at 37 °C with 5% CO<sub>2</sub>.

#### WGCNA and GO enrichment analysis

Gene co-expression networks were constructed using the WGCNA package in R for the GSE25097 dataset, and 2942 differentially expressed genes (DEGs) in 46 samples were selected for the top 50% of the median absolute deviation (MAD), resulting in 1589 genes for subsequent analysis. The soft threshold was determined as 28 ( $R^2=0.9$ ) according to the pickSoftThreshold function, while the weighted adjacency matrix was constructed and transformed into a topological overlap matrix (TOM matrix). Then, hierarchical clustering based on the dissimilarity measure (1-TOM) was performed to identify gene modules, each containing at least 30 genes, and we further set  $abline=0.25$  to merge similar modules. Finally, GO enrichment analysis was performed by combining the target gene's module gene with the corresponding Log<sub>2</sub>FC values of each gene to infer the biological processes in which the gene might be involved.  $P<0.05$  and  $FDR<0.25$  were used as criteria for the genes significant enrichment.

#### Hydroxyproline assay

The hydroxyproline detection kits were purchased from Nan Jing Jian Cheng Biochemical Institute (Nanjing, China). Mouse liver tissues were weighed and disassembled upon request, and the determination of hydroxyproline content in the liver was completed according to the manufacturer's instructions.

#### AST, ALT and LDH assays

AST, ALT and LDH levels in the serum of mice were assessed using commercial assay kits (Nan Jing Jian Cheng, Nanjing, China) according to the manufacturer's instructions.

#### CCK8 assay

Cells were seeded in a 96-well plate at a volume of 90  $\mu$ l of cell culture medium per well. Subsequently, 10  $\mu$ l of CCK8 reagent was added to each well. Then the plate was gently shaken to make the CCK8 reagent evenly distributed in the wells and incubated at 37°C for 1 h. After that, the absorbance was measured at 450 nm, and the absorbance values obtained were analyzed to determine the viability of the cells.

#### Confocal microscopy

The isolated primary HC were evenly spread in collagen-coated 24-well plates, each well containing a 15 mm



diameter circular glass coverslip. Following cell adhesion to the collagen-coated surfaces, the cells were subjected to the designated treatments. The cells were then fixed with a 4% paraformaldehyde tissue fixative for 30 min at room temperature. Subsequently, cell membranes were permeabilized using 1% Triton X-100 for 30 min. After permeabilization, the cells were washed with 1×PBS, incubated with goat serum at 37°C for 30 min and then incubated with p65 antibody (p65, 1:200, mouse monoclonal, Santa Cruz, sc-8008) for 16 h at 4°C. On the following day, the anti-mouse fluorescent secondary antibody (1:1000) was added, incubated for 1 h at room temperature and protected from light. Next, the nuclei were stained with DAPI (1:1000) and incubated for 30 min at room temperature. After washing the culture plate, the small circular slide was removed to the new object slide and placed in the dark box. Finally, the immunofluorescence was visualized by a confocal microscope.

#### Construction of plasmids

The GPR56 overexpression plasmid was constructed using the Seamless Cloning Kit (NCM Biotech, M9001). The CDS region of mouse GPR56 gene was queried by NCBI, and amplification primers were designed based on the 5' and 3' end base sequences of the CDS region (Table S3). The mouse AAV8-TBG-GPR56 plasmid was used for animal experiments, and the mouse 305-GPR56 plasmid was used for subsequent cellular experiments. In addition, the plasmid was constructed using T4 ligase to knock down GPR56. The mouse AAV8-GPR56-shRNA and mouse pLKO.1-GPR56-shRNA interference sequences were constructed, and the former was used for animal experiments and the latter for cellular experiments (Table S3).

#### Lentivirus production

The 293T cells were prepared for lentivirus production when they reached a density of 60–70%. For overexpression, plasmids encoding the viral proteins, including pMDL, pVSVG, and pRev, were utilized. For knockdown experiments, pMD2.G and psPAX2 plasmids were employed. The culture medium containing the target plasmids was mixed with the transfection reagent polyethylenimine (PEI) and incubated for 20 min. Then, the mixture was slowly added to the cell culture medium, and the cells were cultured for 4–6 h and replaced with new culture medium. Finally, the collected medium was centrifuged and filtered through a 0.45 µm filter.

#### Production of AAV8

Transfection was initiated when the density of AAV293 cells reached 70–80% confluency. The target plasmids included AAV8-TBG-GPR56, AAV8-TBG-Ctrl, AAV8-GPR56-shRNA, AAV8-NC, and the helper plasmids

included pAAV2/8 and pAAVΔF6. Then, the target plasmids, helper plasmids and transfection reagent PEI were added to OPTI-MEM and mixed well and incubated for 15 min. Subsequently, the transfection mixture was slowly added to the cell culture medium. After a 6-hour incubation, the medium was replaced with complete culture medium containing 10% inactivated FBS and 1% triple antibiotic mixture. The cells were cultured for an additional 4 days to allow for virus production. The virus particles, both cell-associated and in the supernatant, were harvested, and the viral titer was determined following concentration of the virus using ultracentrifugation. Finally, the virus was then injected into the tail vein of the mouse at a concentration of  $1 \times 10^{12}$  vg/ml, with 100–120 µl per mouse.

#### Statistical analysis

Data were expressed as mean ± SD. All the statistical analyzes were performed with SPSS 13.0 (IBM, Armonk, NY, USA). Statistical analyzes were performed using either Student's t-test (two-group comparison) or one-way analysis of variance (more than two groups) followed by *post hoc* comparison, and differences with  $P < 0.05$  were considered significantly.

#### Data availability

All data generated or analyzed during this study are included in this published article and its supplementary information files.

## Results

### Screening for differentially expressed aGPCRs in liver fibrosis

To identify aGPCRs with altered expression in liver fibrosis, we conducted a search in the GEO database for datasets related to liver fibrosis. We focused our analysis on the gene microarray datasets GSE174099 and GSE25097, applying a cutoff for differential gene expression:  $P_{adj} < 0.05$ ,  $|\log_2 FC| \geq 1$ . These criteria yielded 2577 and 2942 differentially expressed genes for each dataset, respectively (Fig. S1A–D). We then intersected these gene lists with the known 33 aGPCRs, identifying GPR56, GPR64, and GPR126 as candidates of interest (Fig. S1E). Among these, GPR56 was selected for further investigation due to its significant upregulation and the lowest  $P$ -value. Notably, in the GSE25097 dataset, GPR56 showed a  $\log_2 FC$  of 1.3 ( $P_{adj} = 0.00118$ ) in liver tissues from patients with cirrhosis relative to normal subjects (Fig. S1F). Similarly, in the GSE174099 dataset, GPR56 exhibited a  $\log_2 FC$  of 4.1 ( $P_{adj} = 0.00018$ ) in liver tissues from rats subjected to BDL compared to sham controls (Fig. S1G). These data reveal that GPR65 may act as an important molecule in liver fibrosis.

### Expression analysis of GPR56 in mouse and human liver tissue

To detect the expression of GPR56 in fibrotic liver tissue, a liver fibrosis model was induced by intraperitoneal injection of CCl<sub>4</sub> in mice for 6 weeks. Macroscopic examination, HE, Sirius Red, Masson's trichrome staining, IHC for  $\alpha$ -SMA, as well as western blot and qRT-PCR analysis for  $\alpha$ -SMA (*Acta2*), COL1A1 (*Col1a1*), MMP2 (*Mmp2*), and TIMP1 (*Timp1*), which are marker genes for liver fibrosis, were performed to validate the successful establishment of the liver fibrosis models (Fig. 1A-C). Subsequently, GPR56 expression was assessed in fibrotic liver tissues using qRT-PCR, western blot, and IHC, and the results revealed that the expression of GPR56 is significantly increased within the fibrotic livers compared to controls (Fig. 1A-C). Consistent results were obtained from the BDL model (Fig. 1D-F). To further investigate the cellular source of GPR56 upregulation, we isolated HC, HSC, Hepatic macrophage (HM), and liver sinusoidal endothelial cells (LSEC) from both CCl<sub>4</sub>-induced fibrosis model mice and normal mice. qRT-PCR and western blot analysis indicated higher GPR56 expression in HC from the experimental group compared to normal mice, while expression in the other cell types was either reduced or not significantly different (Fig. 1G and H). These findings suggest that the increase of GPR56 during liver fibrosis is primarily attributed to the elevated expression in HC.

Given the potential of GPR56 as a biomarker for clinical assays and a target for therapeutic intervention, we collected normal human liver tissue ( $n=10$ ) and liver tissue from patients with cirrhosis ( $n=20$ ). Western blot and qRT-PCR results indicated elevated expression of GPR56 at both the protein and mRNA levels in liver tissues of patients with cirrhosis (Fig. 2A and B). Furthermore, IHC data demonstrated a significant increase in GPR56-positive areas in cirrhotic liver tissues compared to normal tissues (Fig. 2C). The diagnostic accuracy of GPR56 was assessed using ROC curve analysis based on its mRNA expression levels and clinical diagnosis, which revealed a moderate to high accuracy in identifying the cirrhosis population, with an AUC of 0.895 and a confidence interval (CI) of 0.783 to 1.000 (Fig. 2D). Collectively, these findings substantiate the elevated expression of GPR56 in liver fibrosis and underscore its potential significance in clinical diagnostics.

### WGCNA and GO enrichment analysis

To identify key genes associated with liver fibrosis, we performed WGCNA enrichment analysis on the 2942 differentially expressed genes from the GSE25097 dataset, focusing on the top 50% ranked by median absolute deviation (MAD), which encompassed 1589 genes. Firstly, gene expression patterns categorized the 46 samples into

distinct groups (Fig. S2A). Subsequently, a soft thresholding power of 28, corresponding to an  $R^2$  value of 0.9, was determined to be optimal for constructing a weighted adjacency matrix (Fig. S2B). Finally, the 1589 genes were clustered into three modules: the black, grey, and red modules (Fig. S2C), with GPR56 being a member of the red module. The 745 genes within the red module, along with their Log<sub>2</sub>FC values, were then subjected to GO enrichment analysis. The analysis indicated that the red module genes are predominantly involved in inflammatory responses and the synthesis of the ECM (Fig. S2D and Table S4). Based on these findings, we hypothesize that GPR56 may play a role in the pathogenesis of liver fibrosis by modulating inflammatory responses and ECM synthesis.

### Hepatocyte-specific overexpression of GPR56 attenuates CCl<sub>4</sub> and BDL-induced liver fibrosis and cell pyroptosis

To investigate the function of GPR56 in liver fibrosis, we conducted in vivo experiments involving tail vein injections of either control virus or AAV8 specifically overexpressing GPR56 in HC of mice. Following a one-week viral administration, mice were subjected to intraperitoneal injections of CCl<sub>4</sub> for 6 weeks. qRT-PCR and western blot analyses confirmed significant upregulation of GPR56 in the livers of mice from the AAV8-TBG-GPR56 and AAV8-TBG-GPR56 + CCl<sub>4</sub> groups compared to the control group, indicating successful overexpression of GPR56 (Fig. 3A and B). Furthermore, mice in the CCl<sub>4</sub> group developed severe liver fibrosis which was mitigated by hepatocyte-specific overexpression of GPR56. This alleviation was evidenced by qRT-PCR analysis of *Acta2*, *Col1a1*, *Mmp2*, and *Timp1*, western blot analysis of  $\alpha$ -SMA, MMP2, and TIMP1, macroscopic examination, HE, Sirius Red, Masson's trichrome staining, and IHC for  $\alpha$ -SMA (Fig. 3A-C). Additionally, the reduction in liver fibrosis and injury was corroborated by decreased liver hydroxyproline content as well as serum levels of lactate dehydrogenase (LDH), alanine aminotransferase (ALT), and aspartate aminotransferase (AST) (Fig. 3D-G).

We hypothesized that GPR56 may play a role in cellular pyroptosis associated with liver fibrosis based on GO enrichment analysis. In the CCl<sub>4</sub>-induced liver fibrosis mouse model, pronounced DNA fragmentation was observed. However, hepatocyte-specific overexpression of GPR56 reduced nuclear DNA breaks, as shown by TUNEL staining (Fig. 3H). Consistent with these findings, western blot analysis revealed that CCl<sub>4</sub> treatment significantly increased the protein levels of pyroptosis-associated proteins including NLRP3, GSDMD-N, and cleaved-Caspase1 compared with the control group, while overexpression of GPR56 significantly decreased the CCl<sub>4</sub>-induced upregulation of these proteins (Fig. 3I). qRT-PCR analysis further indicated that forced GPR56

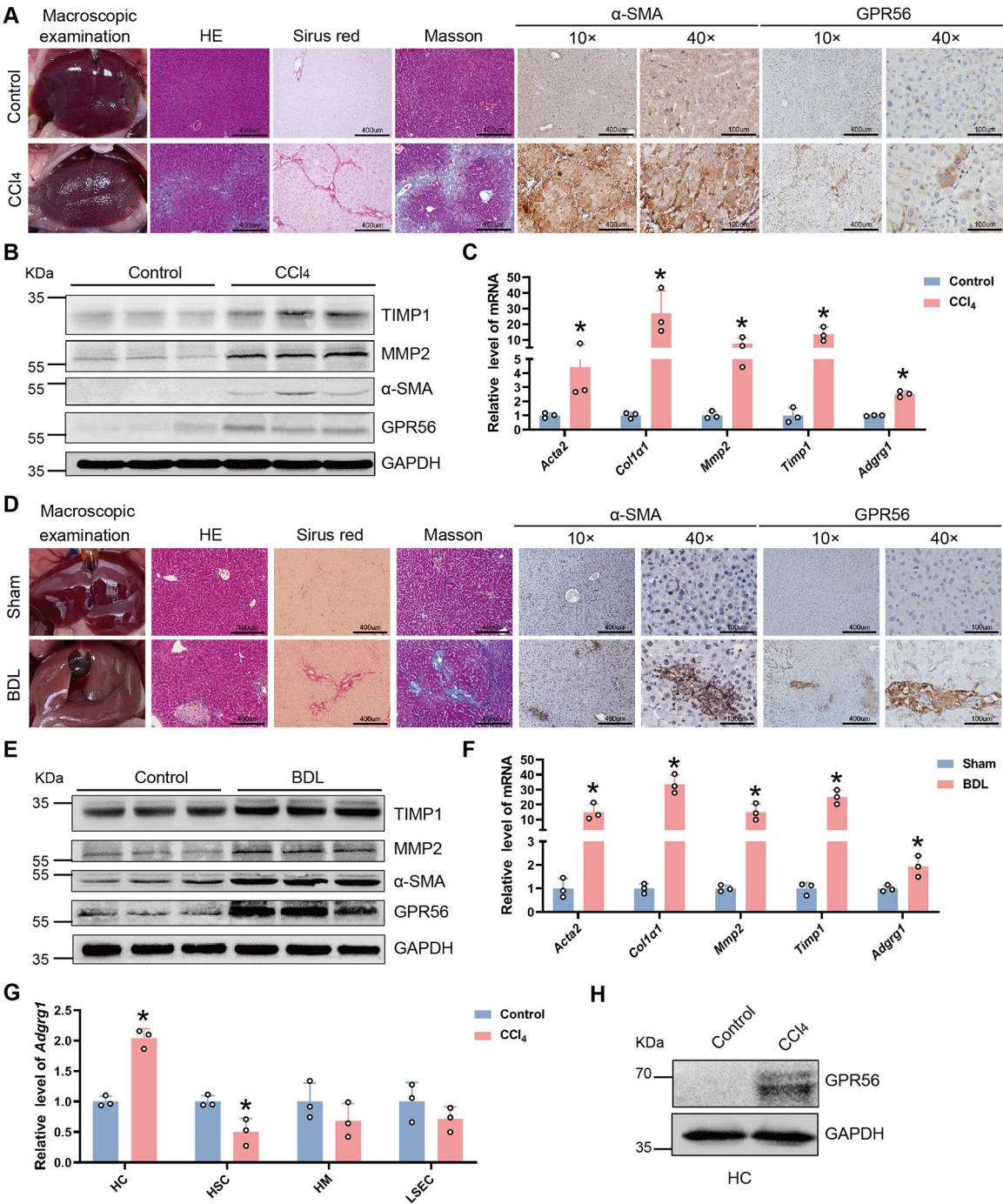


**Fig. 1** GPR56 is increased in mouse fibrotic liver tissues. **(A)** Mouse liver macroscopic examination, HE staining, Sirius red staining, Masson staining, and IHC staining of  $\alpha$ -SMA and GPR56 in the livers of mice treated with or without CCl<sub>4</sub> for 6 weeks. **(B)** The protein level of TIMP1, MMP2,  $\alpha$ -SMA and GPR56 in the livers of mice treated with or without CCl<sub>4</sub> was determined by western blot. GAPDH was used as an internal control. **(C)** The mRNA level of *Acta2*, *Col1a1*, *Mmp2*, *Timp1* and *Adgrg1* in the livers of mice treated with or without CCl<sub>4</sub> was detected by qRT-PCR. **(D)** Mouse liver macroscopic examination, HE staining, Sirius red staining, Masson staining, and IHC staining of  $\alpha$ -SMA and GPR56 in the livers of mice with or without BDL for 21 days. **(E)** The protein level of TIMP1, MMP2,  $\alpha$ -SMA and GPR56 in the livers of mice with or without BDL was determined by western blot. GAPDH was used as an internal control. **(F)** The mRNA level of *Acta2*, *Col1a1*, *Mmp2*, *Timp1* and *Adgrg1* in the livers of mice with or without BDL was detected by qRT-PCR. **(G)** qRT-PCR was used to assess the expression of *Adgrg1* in HC, HSC, HM and LSEC isolated from mice treated with or without CCl<sub>4</sub>. **(H)** The protein level of GPR56 in HC isolated from mice treated with or without CCl<sub>4</sub> was determined by western blot. GAPDH was used as an internal control. \*p < 0.05 vs. Control or Sham



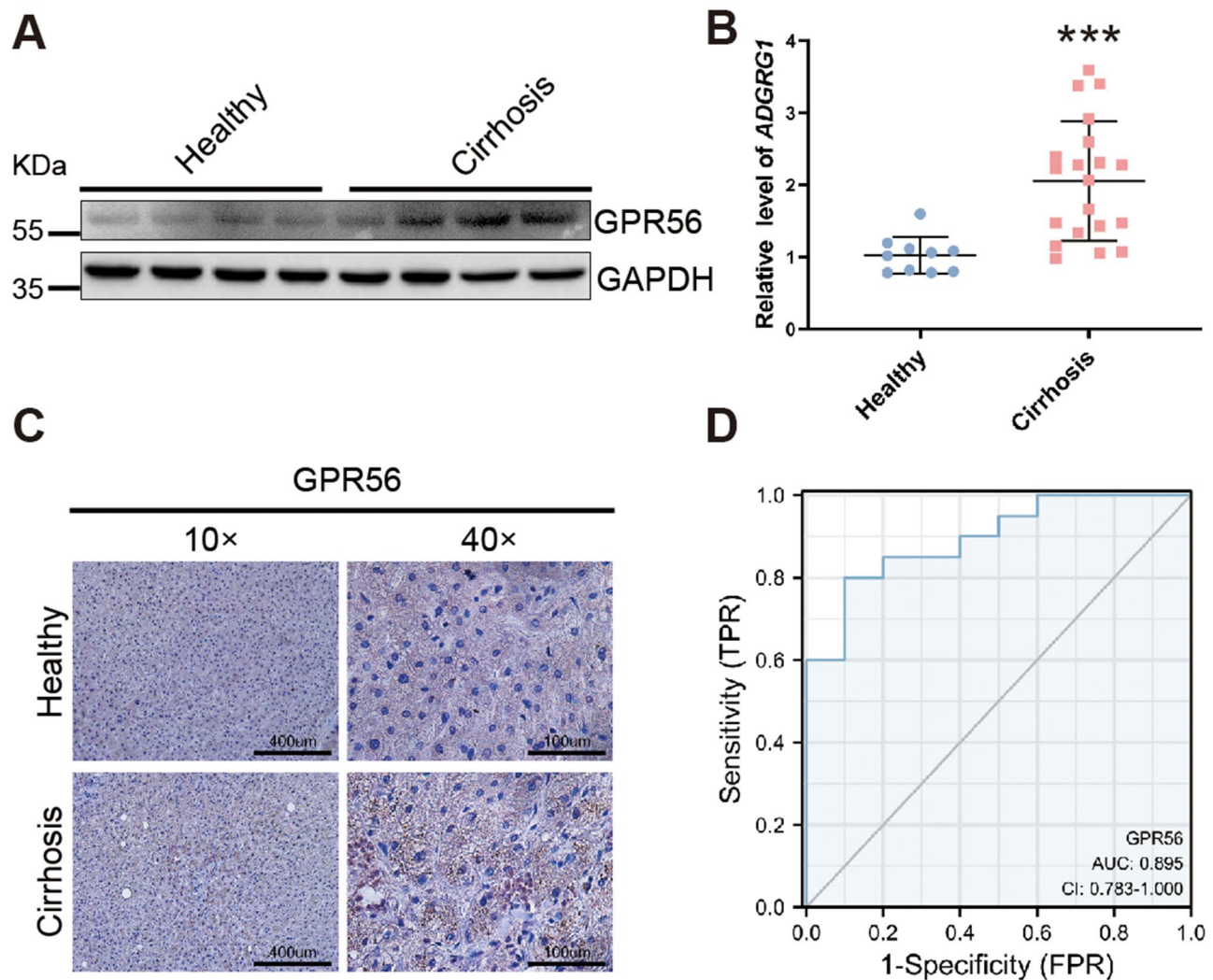


**Fig. 2** GPR56 is elevated in human cirrhotic liver tissues. **(A–C)** The expression of GPR56 in normal human liver tissue ( $n = 10$ ) and liver tissue from patients with cirrhosis ( $n = 20$ ) was determined by western blot, qRT-PCR and IHC. GAPDH was used as an internal control. **(D)** Diagnostic ROC curve of GPR56. \*\*\* $p < 0.001$

expression significantly alleviated  $\text{CCl}_4$ -induced upregulation of pyroptosis-associated genes including *Nlrp3*, *Il1b* and *Il18* (Fig. 3J and K; Fig. S3A).

To exclude the possibility that GPR56 alters the metabolism or toxicity of  $\text{CCl}_4$  rather than directly affecting cell responses, the results were confirmed in a BDL-induced mouse liver fibrosis model. As shown in Fig. 4A–G, mice of BDL group developed severe liver fibrosis and injury, and hepatocyte-specific overexpression of GPR56 inhibited BDL-induced liver fibrosis and injury as demonstrated by qRT-PCR, western blot, macroscopic examination, HE, Sirius Red, Masson's trichrome staining, IHC, as well as measurements of liver hydroxyproline content and serum levels of LDH, ALT and AST level. As expected, overexpression of GPR56 notably alleviated BDL-induced NLRP3 inflammasome-mediated pyroptosis as demonstrated by TUNEL staining, qRT-PCR and

western blot (Fig. 4H–K; Fig. S3B). Collectively, these results suggest that hepatocyte-specific overexpression of GPR56 attenuates  $\text{CCl}_4$  and BDL-induced liver fibrosis and cell pyroptosis.

#### Knockdown of GPR56 exacerbates $\text{CCl}_4$ -induced liver fibrosis and cell pyroptosis

To test whether knockdown of GPR56 would aggravate liver fibrosis and NLRP3 inflammasome-mediated pyroptosis in vivo, AAV8-NC or AAV8-GPR56-shRNA was intravenously injected into the  $\text{CCl}_4$ -treated or oil-treated mice via the tail vein one week before the first injection of  $\text{CCl}_4$ . After 6 weeks of  $\text{CCl}_4$  treatment, qRT-PCR and western blot analysis confirmed that GPR56 was knocked down in the liver fibrosis model (Fig. 5A and B). Moreover, mice in  $\text{CCl}_4$  group developed severe liver fibrosis and injury, and knockdown of GPR56 further aggravated



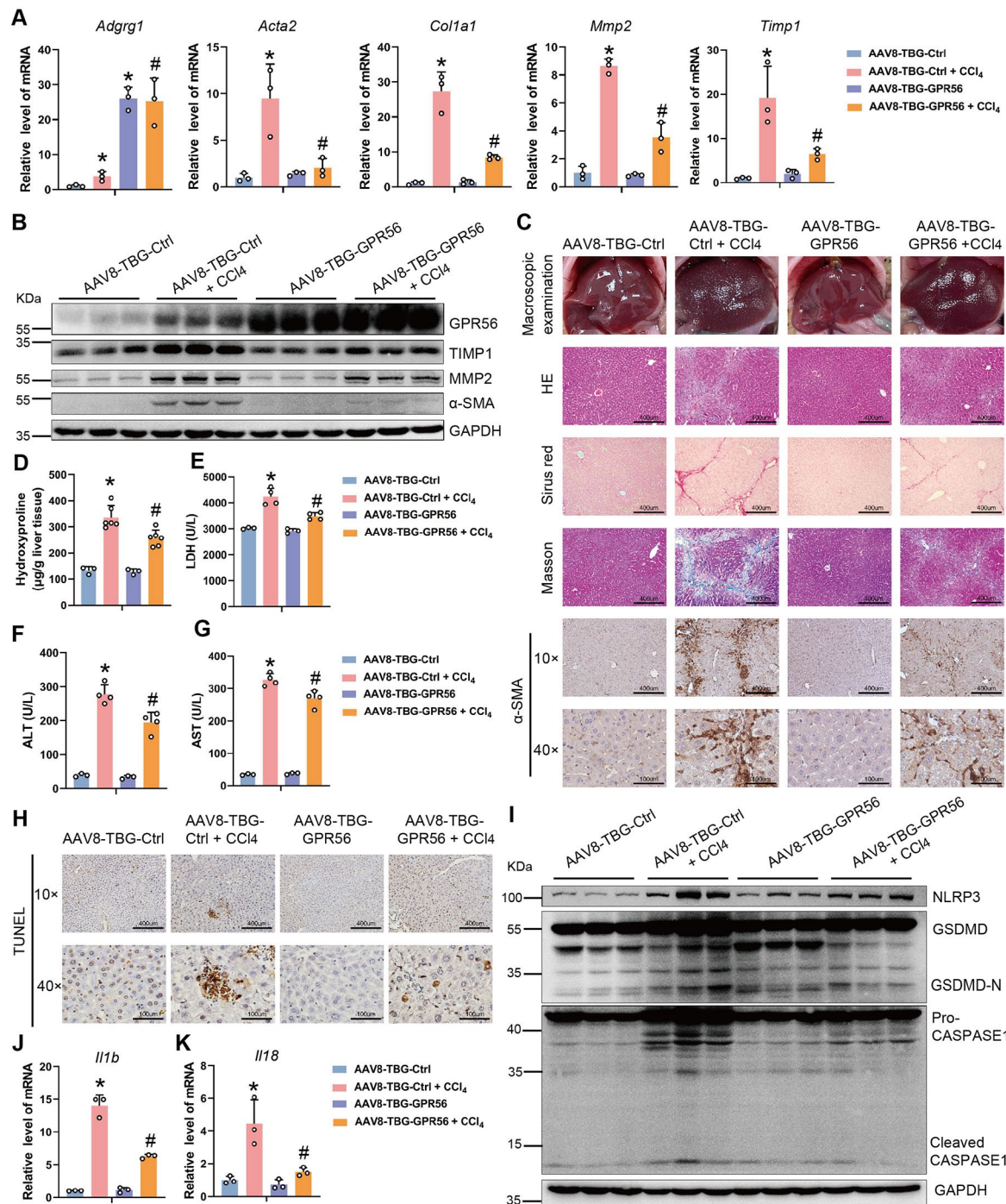


**Fig. 3** Hepatocyte-specific overexpression of GPR56 attenuates CCl<sub>4</sub>-induced liver fibrosis and cell pyroptosis. Balb/c mice were randomly divided into 4 groups: AAV8-TBG-Ctrl group ( $n=6$ ), AAV8-TBG-Ctrl + CCl<sub>4</sub> group ( $n=8$ ), AAV8-TBG-GPR56 group ( $n=6$ ) and AAV8-TBG-GPR56 + CCl<sub>4</sub> group ( $n=8$ ). **(A)** The mRNA level of *Adgrg1*, *Acta2*, *Col1a1*, *Mmp2* and *Timp1* was detected by qRT-PCR. **(B)** The protein level of GPR56, TIMP1, MMP2 and α-SMA was determined by western blot. GAPDH was used as an internal control. **(C)** Mouse liver macroscopic examination, HE, Sirius red and Masson staining of liver tissues and IHC staining of α-SMA. **(D)** The content of hepatic hydroxyproline was quantified. **(E-G)** Serum LDH **(E)**, ALT **(F)**, and AST **(G)** were examined. **(H)** TUNEL staining. **(I)** The protein level of NLRP3, GSDMD and Caspase 1 was determined by western blot. GAPDH was used as an internal control. **(J, K)** The mRNA level of *Il1b* and *Il18* was detected by qRT-PCR. \* $p < 0.05$  vs. AAV8-TBG-Ctrl, # $p < 0.05$  vs. AAV8-TBG-Ctrl + CCl<sub>4</sub>

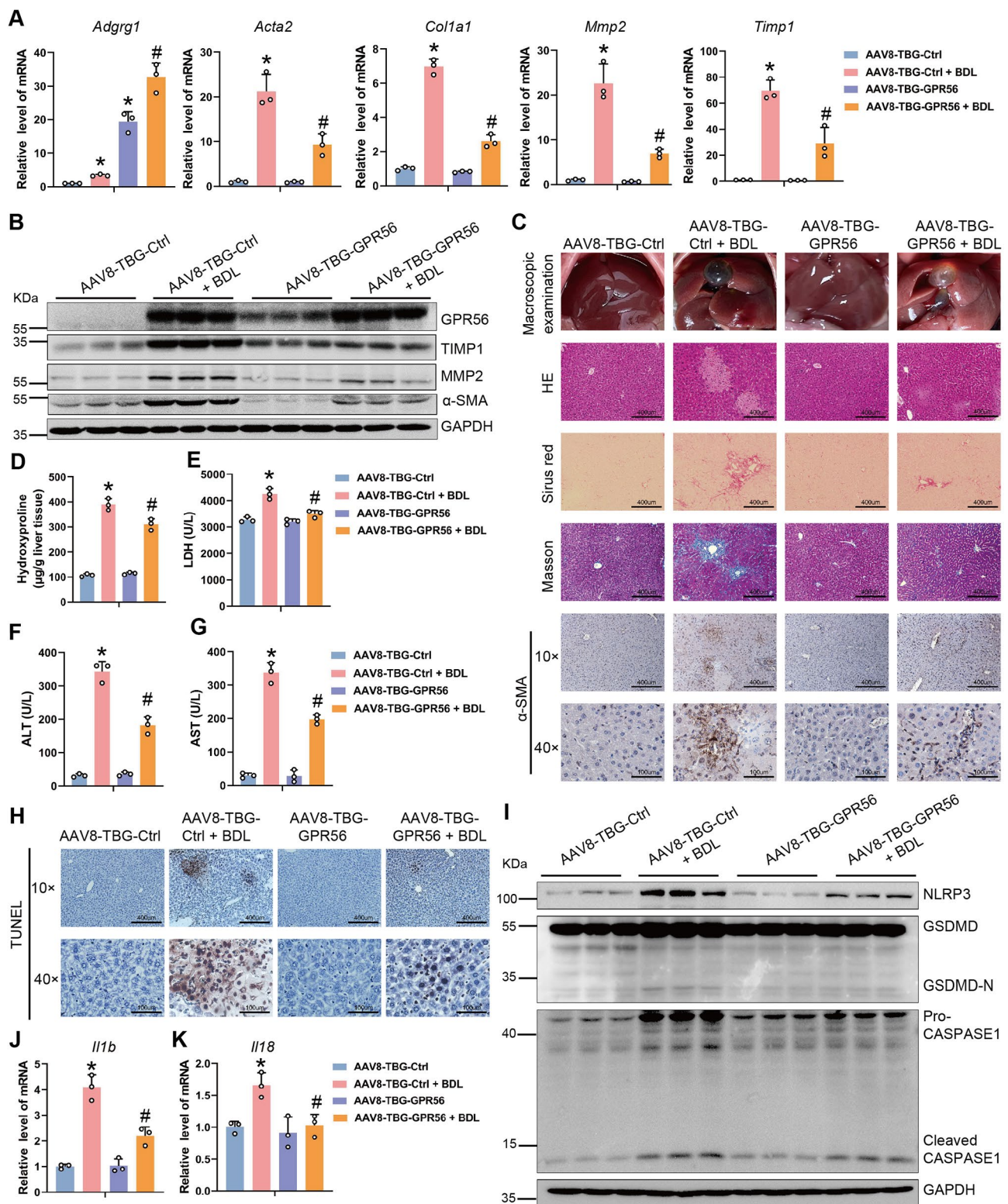


**Fig. 4** Hepatocyte-specific overexpression of GPR56 attenuates BDL-induced liver fibrosis and cell pyroptosis. C57BL/6J mice were randomly divided into 4 groups: AAV8-TBG-Ctrl group ( $n=6$ ), AAV8-TBG-Ctrl+BDL group ( $n=10$ ), AAV8-TBG-GPR56 group ( $n=6$ ) and AAV8-TBG-GPR56 + BDL group ( $n=10$ ). (A) The mRNA level of *Adgrg1*, *Acta2*, *Col1a1*, *Mmp2* and *Timp1* was detected by qRT-PCR. (B) The protein level of GPR56, TIMP1, MMP2 and  $\alpha$ -SMA was determined by western blot. GAPDH was used as an internal control. (C) Mouse liver macroscopic examination, HE, Sirius red and Masson staining of liver tissues and IHC staining of  $\alpha$ -SMA. (D) The content of hepatic hydroxyproline was quantified. (E-G) Serum LDH (E), ALT (F), and AST (G) were examined. (H) TUNEL staining. (I) The protein level of NLRP3, GSDMD and Caspase 1 was determined by western blot. GAPDH was used as an internal control. (J, K) The mRNA level of *Il1b* and *Il18* was detected by qRT-PCR. \* $p < 0.05$  vs. AAV8-TBG-Ctrl, # $p < 0.05$  vs. AAV8-TBG-Ctrl + BDL.



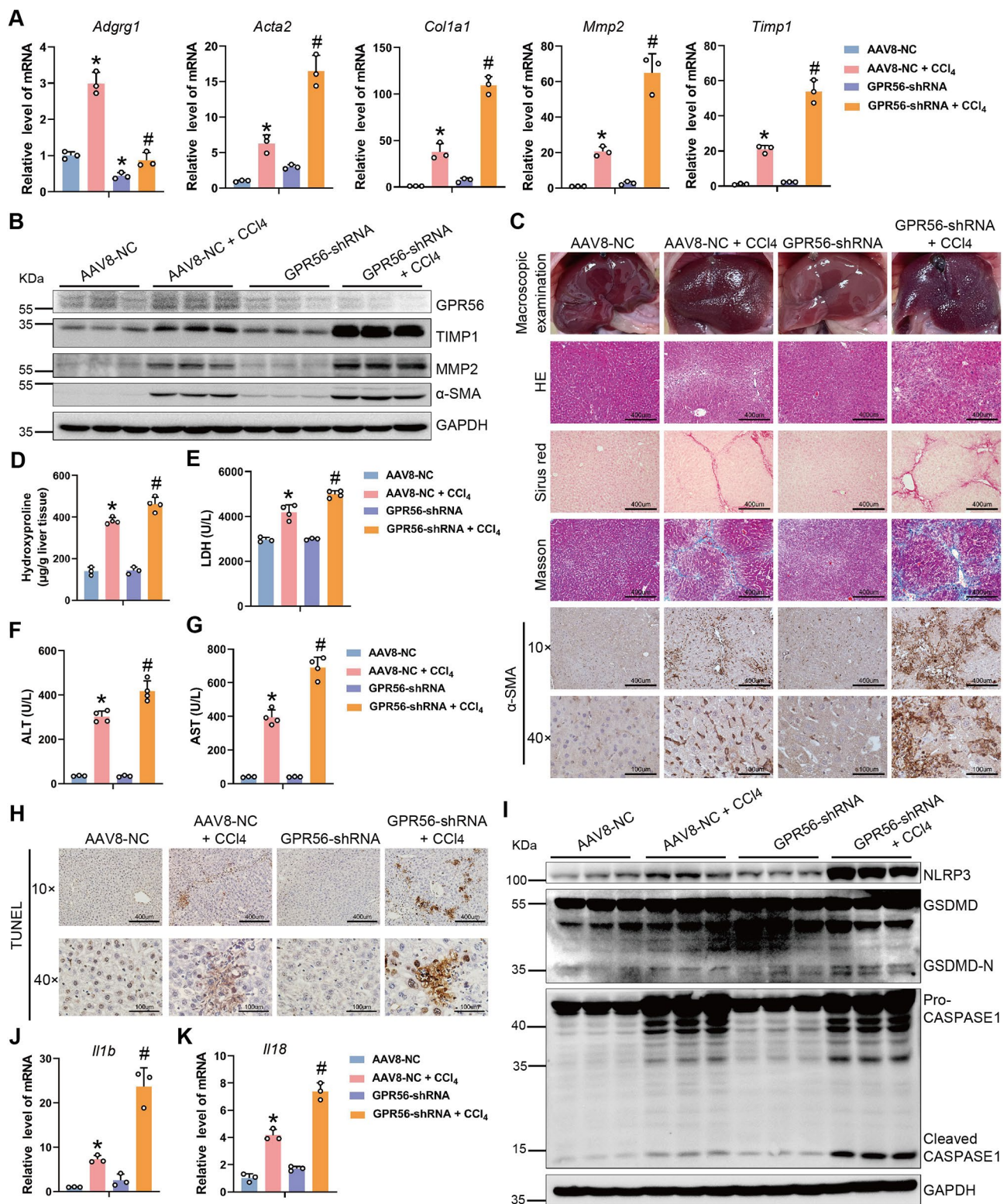


**Fig. 5** Knockdown of GPR56 exacerbates CCl<sub>4</sub>-induced liver fibrosis and cell pyroptosis. Balb/c mice were randomly divided into 4 groups: AAV8-NC group (n=6), AAV8-NC + CCl<sub>4</sub> group (n=8), GPR56-shRNA group (n=6) and GPR56-shRNA + CCl<sub>4</sub> group (n=8). **(A)** The mRNA level of *Adgrg1*, *Acta2*, *Col1a1*, *Mmp2* and *Timp1* was detected by qRT-PCR. **(B)** The protein level of GPR56, TIMP1, MMP2 and α-SMA was determined by western blot. GAPDH was used as an internal control. **(C)** Mouse liver macroscopic examination, HE, Sirius red and Masson staining of liver tissues and IHC staining of α-SMA. **(D)** The content of hepatic hydroxyproline was quantified. **(E-G)** Serum LDH **(E)**, ALT **(F)**, and AST **(G)** were examined. **(H)** TUNEL staining. **(I)** The protein level of NLRP3, GSDMD and Caspase 1 was determined by western blot. GAPDH was used as an internal control. **(J, K)** The mRNA level of *Il1b* and *Il18* was detected by qRT-PCR. \*p < 0.05 vs. AAV8-NC, #p < 0.05 vs. AAV8-NC + CCl<sub>4</sub>.



$\text{CCl}_4$ -induced liver fibrosis and injury as demonstrated by qRT-PCR, western blot, macroscopic examination, HE, Sirius Red, Masson's trichrome staining, IHC, as well as measurements of liver hydroxyproline content and serum levels of LDH, ALT and AST level (Fig. 5A-G). In addition, deletion of GPR56 notably promoted  $\text{CCl}_4$ -induced NLRP3 inflammasome-mediated pyroptosis as demonstrated by TUNEL staining, qRT-PCR and western blot (Fig. 5H-K; Fig. S3C). Collectively, these results suggest that GPR56 deficiency aggravates  $\text{CCl}_4$ -induced liver fibrosis and cell pyroptosis.

#### **GPR56 inhibits LPS/Nigericin-induced hepatocyte pyroptosis**

To investigate the role and effect of GPR56 on HC pyroptosis *in vitro*, we isolated mouse primary HC and established a HC pyroptosis model using LPS/Nigericin (Nig). The successful construction of the HC pyroptosis as demonstrated by reduced cell proliferation ability, elevated LDH in the supernatant, increased cleaved-Caspase1 and GSDMD-N protein level as well as upregulated *Nlrp3* and *Il1b* RNA level (Fig. S4A-D). Western blot and qRT-PCR results suggested that the expression of GPR56 was significantly higher in the LPS/Nig-treated group compared to the LPS or Control groups (Fig. S4C and D). To further examine the role of GPR56 in HC pyroptosis, we overexpressed GPR56 in HC followed by LPS/Nig treatment. qRT-PCR and western blot results revealed that GPR56 was significantly overexpressed in the Lenti-GPR56 group compared to the Lenti-Control group, at both mRNA and protein levels, indicating successful overexpression in HC (Fig. 6A and B). Moreover, the mRNA level of the pyroptosis-related genes *Nlrp3* and *Il1b* was upregulated upon LPS/Nig treatment, but this upregulation was inhibited by forced GPR56 expression (Fig. 6A). Western blot results also showed that LPS/Nig treatment significantly upregulated the protein level of cleaved-Caspase1 and GSDMD-N, while GPR56 overexpression significantly abrogated LPS/Nig-induced upregulation of these proteins (Fig. 6B). We also detected the cell proliferation ability by CCK8. As expected, the results revealed that overexpression of GPR56 diminished the reduction in cell proliferation ability induced by LPS/Nig (Fig. 6C). Similarly, forced GPR56 expression attenuated LPS/Nig-induced LDH release (Fig. 6D). On the other hand, knockdown of GPR56 significantly promoted the mRNA level of *Nlrp3* and *Il1b*, the protein level of cleaved-Caspase1 and GSDMD-N, the release of LDH as well as the cell proliferation inhibition, in both LPS/Nig-treated and untreated conditions (Fig. 6E-H). Taken together, the results suggest that overexpression of GPR56 attenuates HC pyroptosis, while knockdown of GPR56 has the opposite effect.

#### **GPR56 inhibits HSC activation indirectly through the signals derived from hepatocyte**

HC damage or death is widely acknowledged as a pivotal initiator of fibrosis in the context of ongoing hepatic injury [30]. Hence, conditional medium (CM) from control or GPR56-silenced HC in the presence or absence of LPS/Nig were used to incubate mouse primary HSC. The results revealed that treatment with the CM from LPS/Nig-treated HC markedly promoted the expression of the pro-fibrotic genes, suggesting that the factors released during HC pyroptosis activate HSC, leading to the increased synthesis of ECM (Fig. 6I; Fig. S5A and B). However, this effect was negated by overexpression of GPR56 in hepatocytes (Fig. S5A and B). On the other hand, qRT-PCR results showed that knockdown of GPR56 in HC, irrespective of LPS/Nig treatment, promoted the mRNA level of *Acta2*, *Col1a1*, *Mmp2* and *Timp1* (Fig. 6I). Consistently, western blot further confirmed that CM from GPR56-silenced HC markedly promoted the expression of COL1 $\alpha$ 1 and  $\alpha$ -SMA in HSC (Fig. 6J). Taken together, the results show that knockdown of GPR56 in HC activates HSC and enhances ECM synthesis.

#### **GPR56 inhibits HC pyroptosis through the NF- $\kappa$ B pathway**

The NF- $\kappa$ B signaling pathway is recognized for its significant role in cellular pyroptosis and the progression of liver fibrosis [29, 33]. To verify whether GPR56 is involved in the regulation of the NF- $\kappa$ B pathway, we initially measured the level of total and phosphorylated forms of IKK, p65 and I $\kappa$ B in liver tissues from control, GPR56-overexpressed, GPR56-silenced mice with or without induction of fibrosis by  $\text{CCl}_4$ /BDL. The results showed that mice treated with  $\text{CCl}_4$ /BDL exhibited increased levels of phos-IKK, phos-I $\kappa$ B and phos-p65, with no significant changes in total protein levels (Fig. S6A-C). Notably, hepatocyte-specific overexpression of GPR56 attenuates  $\text{CCl}_4$  and BDL -induced phosphorylation of IKK, I $\kappa$ B and p65, while knockdown of GPR56 significantly enhanced  $\text{CCl}_4$ -induced the activation of NF- $\kappa$ B pathway (Fig. S6A-C). Furthermore, western blot analysis revealed that LPS/Nig treatment substantially induced the phosphorylation of IKK, p65, and I $\kappa$ B $\alpha$ , an effect that was attenuated by the overexpression of GPR56 in primary HC (Fig. 7A). Confocal microscopy further demonstrated that LPS/Nig treatment facilitated the nuclear translocation of p65, while forced GPR56 expression significantly attenuated LPS/Nig-induced p65 translocation (Fig. 7B). Conversely, knockdown of GPR56 promoted the phosphorylation and nucleus translocation of p65, which is abrogated by the specific inhibitors of NF- $\kappa$ B BAY11-7082 (Fig. 7C and D). Meanwhile, western blot results revealed that BAY11-7082 abrogated the upregulation of GSDMD-N induced by GPR56 deficiency (Fig. 7E), and qRT-PCR confirmed

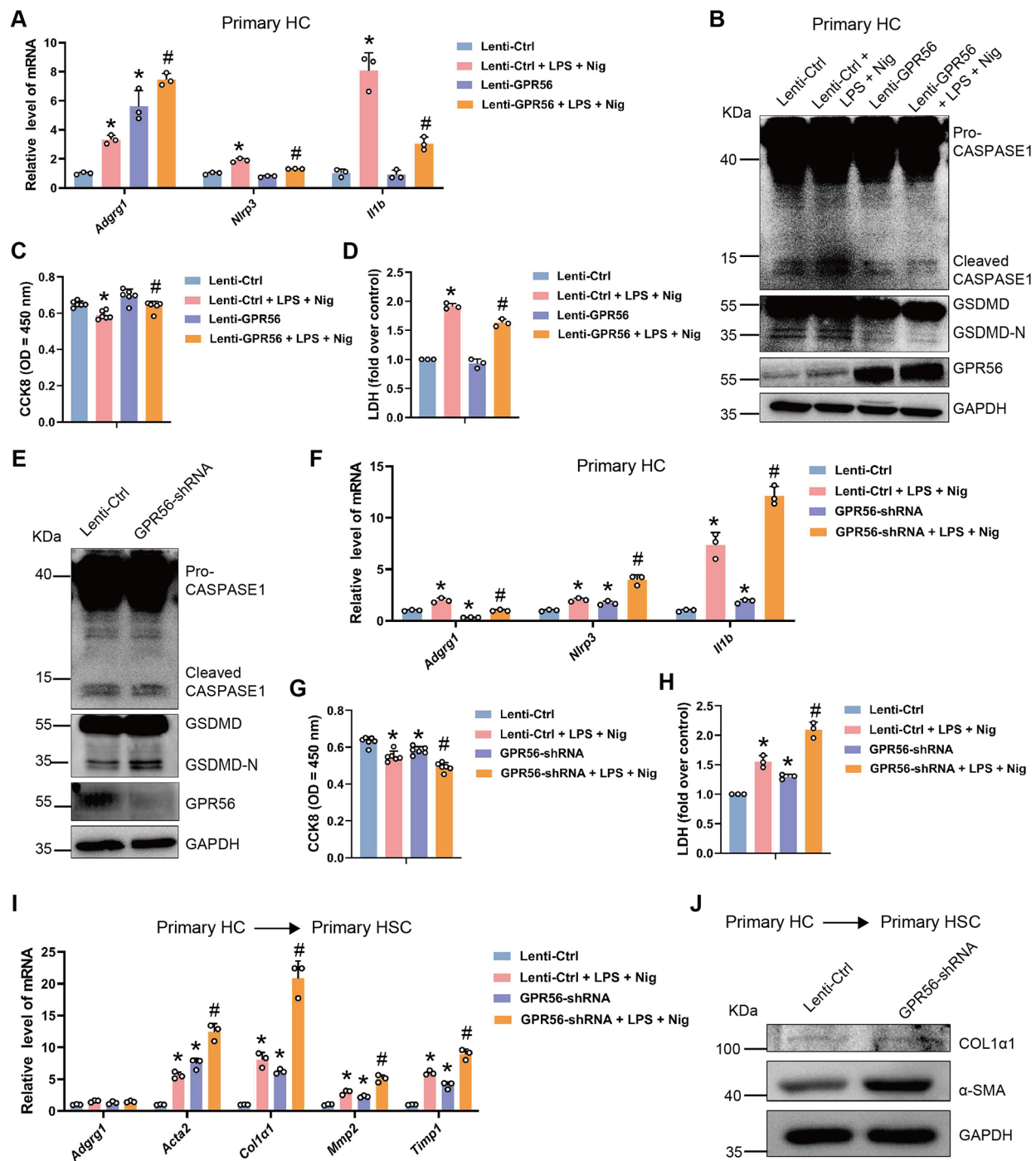


**Fig. 6** GPR56 inhibits LPS/Nigericin-induced hepatocyte pyroptosis. **(A–D)** Primary HC were infected with lentivirus-mediated control or GPR56 for 72 h, then these cells were stimulated with 100 ng/ml LPS for 4 h and subsequently treated them with 100ng/ml for 2 h. The mRNA level of *Adgrg1*, *Nlrp3* and *Il1b* was detected by qRT-PCR **(A)**; the protein level of GPR56, GSDMD and Caspase 1 was determined by western blot **(B)**. GAPDH was used as an internal control. Cell proliferation ability was assessed by CCK8 **(C)**; pyroptosis was measured by supernatant LDH activity **(D)**. **(E)** Primary HC were infected with lentivirus-mediated control or GPR56-shRNA for 72 h, the protein level of GPR56, GSDMD and Caspase 1 was determined by western blot. GAPDH was used as an internal control. **(F–H)** Primary HC were infected with lentivirus-mediated control or GPR56-shRNA for 72 h, then these cells were stimulated with 100 ng/ml LPS for 4 h and subsequently treated them with 100ng/ml for 2 h. The mRNA level of *Adgrg1*, *Nlrp3* and *Il1b* was detected by qRT-PCR **(F)**; cell proliferation ability was assessed by CCK8 **(G)**; pyroptosis was measured by supernatant LDH activity **(H)**. **(I, J)** The conditional medium (CM) from control or GPR56-silenced HC in the presence or absence of LPS/Nig were used to incubate mouse primary HSCs for 24 h. The mRNA level of *Adgrg1*, *Acta2*, *Col1a1*, *Mmp2* and *Timp1* was detected by qRT-PCR **(I)**; the protein level of COL1a1 and α-SMA was determined by western blot **(J)**. GAPDH was used as an internal control. \* $p < 0.05$  vs. Lenti-Ctrl, # $p < 0.05$  vs. Lenti-Ctrl + LPS + Nig

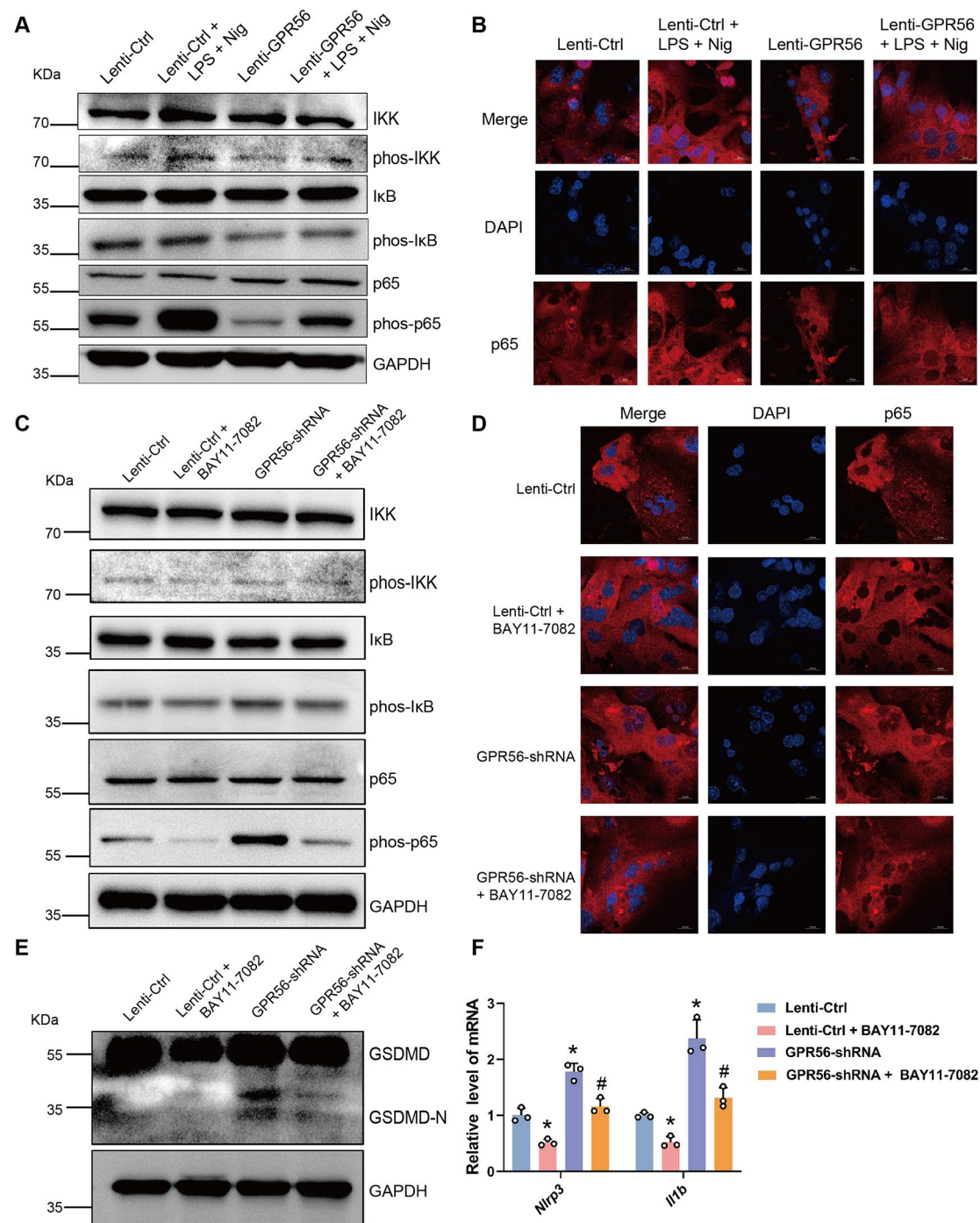


**Fig. 7** GPR56 inhibits HC pyroptosis through the NF- $\kappa$ B pathway. **(A, B)** Primary HC were infected with lentivirus-mediated control or GPR56 for 72 h, then these cells were stimulated with 100 ng/ml LPS for 4 h and subsequently treated them with 100ng/ml for 2 h. The protein level of IKK, phos-IKK, I $\kappa$ B, phos-I $\kappa$ B, p65 and phos-p65 was determined by western blot **(A)**. GAPDH was used as an internal control. The expression and location of p65 was determined by confocal analysis **(B)**; scale bar = 10  $\mu$ m. **(C-F)** 5  $\mu$ mol/L BAY 11-7082 was used to treat GPR56-silenced primary HC for 24 h, the protein level of IKK, phos-IKK, I $\kappa$ B, phos-I $\kappa$ B, p65 and phos-p65 was determined by western blot **(C)**. GAPDH was used as an internal control. The expression and location of p65 was determined by confocal analysis **(D)**; scale bar = 10  $\mu$ m. The protein level of GSDMD was determined by western blot **(E)**. GAPDH was used as an internal control. The mRNA level of *Nlrp3* and *Il1b* was detected by qRT-PCR **(F)**. \* $p$  < 0.05 vs. Lenti-Ctrl, # $p$  < 0.05 vs. GPR56-shRNA



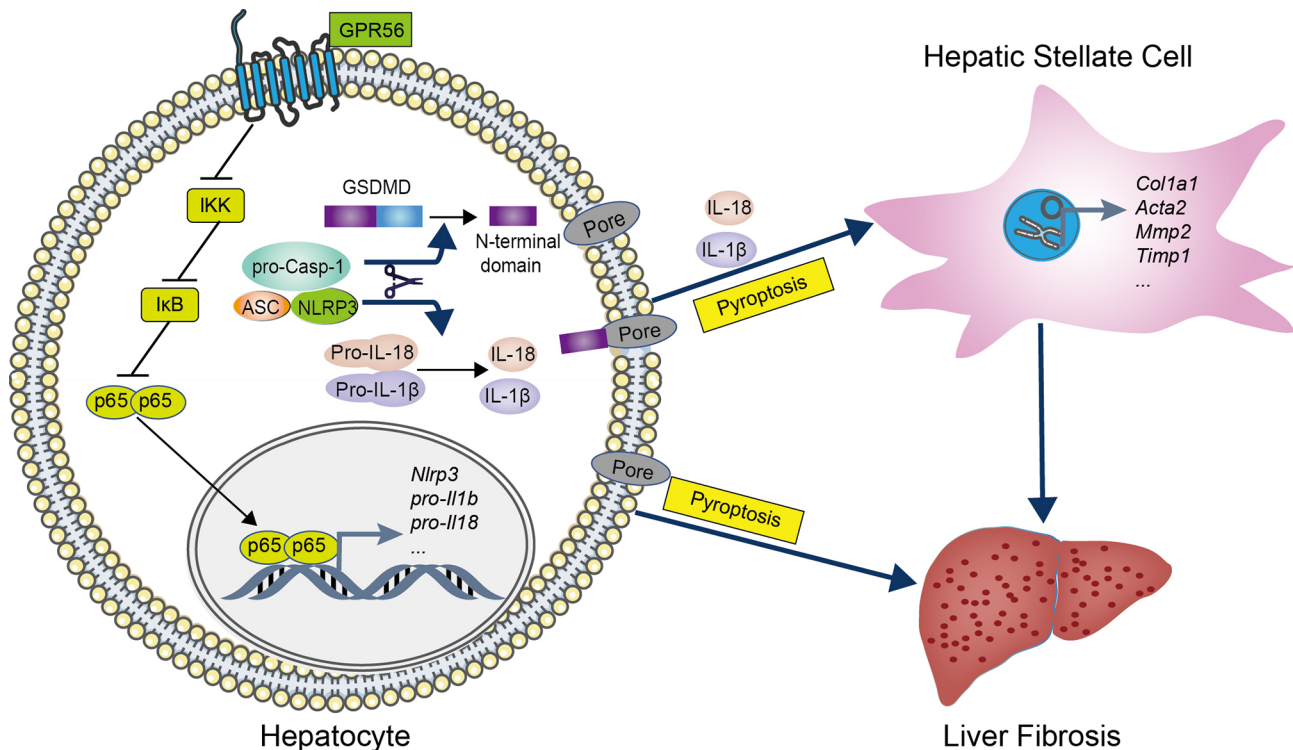


**Fig. 8** Schematic diagram illustrates the role of GPR56 during liver fibrosis

that the NF- $\kappa$ B inhibitor reversed the increased mRNA level of *Nlrp3* and *Il-1b* induced by GPR56 deficiency (Fig. 7F). Taken together, the results suggest that GPR56 inhibits the activation of NF- $\kappa$ B pathway, which in turn suppresses HC pyroptosis (Fig. 8).

## Discussion

Adhesion G protein-coupled receptors (aGPCRs) constitute a distinct subclass within the GPCR family, characterized by an elongated extracellular N terminus that encompasses a GPCR autoproteolysis-inducing (GAIN) domain, which includes a highly conserved GPCR proteolytic site (GPS) [34]. This site can undergo autoproteolysis, resulting in the formation of the N-terminal fragment (NTF) and C-terminal fragment (CTF). Even after cleavage, the NTF and CTF remain associated with the cell membrane in a non-covalent manner until receptor activation. Due to their large NTF, aGPCRs play a crucial role in the interactions between cells and ECM [34]. Additionally, emerging evidence has highlighted the involvement of aGPCRs in the pathogenesis of various diseases, where they exert regulatory effects on cellular processes such as proliferation and senescence [34, 35]. Therefore, identifying aGPCRs that play a significant role in liver fibrosis may provide potential therapeutic targets for the disease. In this study, we identified GPR56, one of the 33 aGPCRs, as upregulated in both mouse and human fibrotic liver tissues, as well as in hepatocytes

from liver fibrosis mice. ROC analysis showed high diagnostic accuracy for cirrhosis. Moreover, hepatocyte-specific overexpression of GPR56 attenuated, while knockdown of GPR56 exacerbated liver fibrosis, suggesting its potential as a new diagnostic and therapeutic target for this condition.

The pathogenesis of liver fibrosis is complex, encompassing cellular and molecular mechanisms. At the cellular level, liver fibrosis is primarily associated with an imbalance between ECM synthesis and degradation, with activated HSC being recognized as the principal drivers of ECM accumulation, a hallmark of liver fibrosis [2, 36, 37]. Additionally, studies have shown that HM and LSEC can also contribute to the regulation of liver fibrosis by secreting cytokines that modulate HSC activation [28, 38]. Hepatocytes, the most abundant cell type in the liver, accounting for 80% of the total liver cell population, have been increasingly studied in recent years for their role in liver fibrosis. The proliferation, apoptosis, and necrosis of hepatocytes play a crucial role in regulating liver fibrosis [30, 39]. Our study revealed that the elevated expression of GPR56 in fibrotic liver tissues was primarily attributed to the increased expression of GPR56 in injured HC, suggesting that the potential impact of GPR56 on liver fibrosis is through its effects on HC damage and warrants further investigation.

HC damage represents one of the pivotal aspects of both chronic and acute liver diseases, with inflammatory

responses also participating and influencing liver pathologies [30, 40]. Pyroptosis, a novel form of inflammatory cell death, primarily relies on the activation of Caspase-1 and the pore-forming action of GSDMD on the cell membrane, leading to the release of intracellular inflammation-associated proteins [41, 42]. Inflammasomes, cytoplasmic multi-protein complexes, are primarily composed of NLRP3, ASC, and pro-Caspase 1. Upon cellular exposure to external stimuli, NLRP3 interacts with ASC to activate caspase-1, which subsequently triggers the maturation of pro-inflammatory cytokines IL-1 $\beta$  and IL-18 and mediates the cleavage of the pore-forming protein GSDMD through proteolytic action, thereby inducing pyroptosis [43, 44]. Although pyroptosis has been extensively studied in immune cells such as macrophages, and our previous work revealed that lnc-LFAR1 exacerbates liver fibrosis by promoting hepatic macrophage pyroptosis [29, 41], emerging evidence suggests that non-immune cells like HC also play a key role in liver fibrosis through pyroptotic pathways [43, 44]. Notably, HC pyroptosis has been reported to activate HSC and enhance ECM deposition, thereby accelerating liver fibrosis progression [45]. Thus, exploring key molecules that regulate HC pyroptosis is crucial for preventing and treating liver fibrosis. In this study, we demonstrated that hepatocyte-specific GPR56 overexpression inhibited CCl<sub>4</sub> and BDL-induced liver fibrosis and cellular pyroptosis, whereas GPR56 knockdown had the opposite effect. To mechanistically investigate GPR56's role in modulating HC pyroptosis, we established an in vitro model using LPS/nigericin (Nig) co-treatment, where Nig specifically activates the NLRP3 inflammasome to potentiate pyroptotic cell death. Remarkably, our in vitro experiments revealed that GPR56 overexpression consistently suppressed pyroptosis and improved hepatocyte viability regardless of LPS/Nig stimulation, while simultaneously inhibiting HSC activation in a paracrine manner. Conversely, GPR56 knockdown exacerbated these effects. These in vivo and in vitro experiments confirm that GPR56 inhibits liver fibrosis and HC pyroptosis, identifying it as a novel pyroptosis regulator and a potential therapeutic target for inflammatory diseases, including liver fibrosis.

Liver fibrosis is a complex process regulated by the interplay of multiple signaling pathways, including the TGF- $\beta$ , NOTCH, Hippo, PI3K-Akt, and NF- $\kappa$ B pathways [30–32, 36, 37, 46]. Notably, the NF- $\kappa$ B pathway is particularly critical in the pathogenesis of liver fibrosis [38, 47]. In its inactive state, the NF- $\kappa$ B complex, comprising p65 and p50 subunits, is sequestered in the cytoplasm by binding to I $\kappa$ B. Activation of IKK leads to the phosphorylation of I $\kappa$ B, which then dissociates from the p65/p50 complex, allowing it to translocate to the nucleus. Once localized to the nucleus, the activated p65 and p50 bind

to specific DNA sequences, initiating the transcription of target genes, including NLRP3, which is a key target gene for NF- $\kappa$ B regulation [29, 48]. Based on these insights, we hypothesized that GPR56 might suppress liver fibrosis and HC pyroptosis by inhibiting the NF- $\kappa$ B pathway. Our data indicated that GPR56 overexpression can indeed suppress the activation of NF- $\kappa$ B pathway and the nuclear translocation of p65. In addition, the rescue experiments further revealed that HC pyroptosis and NF- $\kappa$ B pathway activation in GPR56-silenced primary HC could be attenuated by BAY11-7082, thereby providing stronger evidence that GPR56 inhibits hepatocyte pyroptosis via the NF- $\kappa$ B pathway, further demonstrating that GPR56 could inhibit HC pyroptosis through the NF- $\kappa$ B pathway.

While this study elucidates the crucial role of GPR56 in suppressing HC pyroptosis and liver fibrosis, several limitations should be acknowledged. Firstly, regarding clinical translation, our findings require validation in larger patient cohorts. Future studies should expand the scope of clinical samples to further validate the reliability and accuracy of GPR56 as a diagnostic and prognostic biomarker. Additionally, the proteolytic fragments of GPR56 (NTF/CTF) may represent more suitable serum biomarkers than the full-length protein, and further investigation is needed to explore their detection performance and clinical application value. Secondly, although our study has established GPR56 as a suppressor of HC pyroptosis and liver fibrosis, we have not delved into the development and screening of exogenous or endogenous GPR56 agonists. The specific therapeutic effects and safety of these agonists in liver fibrosis treatment remain to be elucidated and require extensive further research to fully exploit the potential applications of GPR56 in liver fibrosis therapy.

## Conclusions

Our results provide convincing evidence that GPR56 acts as a major repressor of HC pyroptosis and liver fibrosis, thus identifying it as a new potential target for diagnosis and treatment of this condition.

## Abbreviations

GEO	Gene Expression Omnibus
CCl <sub>4</sub>	Carbon Tetrachloride
BDL	Bile Duct Ligation
ECM	Extracellular Matrix
HSC	Hepatic Stellate Cells
HC	Hepatocyte
HM	Hepatic Macrophage
LSEC	Liver Sinusoidal Endothelial Cells
GPCR	G Protein Coupled Receptor
BFPP	Bilateral Frontoparietal Polymicrogyria
OPC	Oligodendrocyte Precursor Cell
IL	Interleukin
LDH	Lactate Dehydrogenase
ALT	Alanine Aminotransferase
AST	Aspartate Aminotransferase
qRT-PCR	quantitative Real-Time Polymerase Chain Reaction

ROC Receiver Operating Characteristic  
Nig Nigercin  
CM Conditional Medium

## Supplementary Information

The online version contains supplementary material available at <https://doi.org/10.1186/s12967-025-06619-8>.

Supplementary Material 1: Additional file 1: figure S1. Differentially expressed aGPCRs in liver fibrosis. Figure S2. WGCNA and GO enrichment analysis. Figure S3. Knockdown of GPR56 exacerbates NLRP3 inflammasome-mediated pyroptosis. Figure S4. GPR56 is increased in LPS/Nigercin-induced hepatocyte pyroptosis. Figure S5. GPR56 inhibits HSC activation indirectly through the signals derived from hepatocyte. Figure S6. GPR56 inhibits the activation of NF- $\kappa$ B pathway. Table S1. Details of GEO series included in this research. Table S2. Primers for plasmid construction. Table S3. qRT-PCR primers for analysis of transcript levels. Table S4. Details information of GO enrichment analysis.

## Acknowledgements

Not applicable.

## Author contributions

Conceptualization, Z.S., Q.L., K.Z., W.H., and T.H.; Methodology, Z.S., Q.L., M.Z., and X.D.; Investigation, Z.S., Q.L., M.Z., X.D., Y.H., and L.Z.; Writing – Original Draft, Q.L. and K.Z.; Writing – Review & Editing, All authors; Funding Acquisition, K.Z., W.H., and T.H.; Supervision, K.Z., W.H., and T.H.

## Funding

This work was supported by the National Natural Science Foundation of China (No. 32171125; 82170630; 82470660; 32200938; 81971331) and Tianjin Natural Science Foundation (No. 22JCZDJC00520; 23JCQNJC00400).

## Data availability

The datasets used and/or analyzed during the current study are available from the corresponding author on reasonable request.

## Declarations

### Ethics approval and consent to participate

The experimental protocol involving mice was formally approved by the Animal Care and Use Committee of Tianjin Medical University to ensure strict adherence to the highest ethical principles and regulatory guidelines.

### Consent for publication

All authors approved the manuscript and gave their consent for submission and publication.

### Competing interests

The authors have declared that no conflict of interest exists.

### Author details

<sup>1</sup>Department of Histology and Developmental Biology, School of Basic Medical Sciences, Tianjin Medical University, No. 22 Qixiangtai Road, Tianjin 300070, China

<sup>2</sup>Department of Hepatology and Gastroenterology, Tianjin Union Medical Center, Tianjin Medical University, Tianjin Union Medical Center Affiliated to Nankai University, No. 190 Jieyuan Road, Tianjin 300121, China

Received: 5 March 2025 / Accepted: 15 May 2025

Published online: 06 June 2025

## References

1. Horn P, Tacke F. Metabolic reprogramming in liver fibrosis. *Cell Metab*. 2024;36:1439–55.

2. Akkiz H, Gieseler RK, Canbay A. Liver fibrosis: from basic science towards clinical progress, focusing on the central role of hepatic stellate cells. *Int J Mol Sci* 2024, 25.
3. Wang T, Liu B, Huang J, Zhao Q, Shen H, Bi T, Liu Z, Dai Y, Sun Q. IFN-gamma-mediated Inhibition of JAK/STAT signaling via nano-scutellarin treatment is an efficient strategy for ameliorating liver fibrosis. *J Transl Med*. 2025;23:195.
4. Xie Y, Yao J, Yan M, Lin Y, Wei J, Wang H, Mao Y, Liu P, Li X. Pretreatment of UC-MSCs with IFN- $\alpha$ 2 improves treatment of liver fibrosis by recruiting neutrophils. *J Transl Med*. 2023;21:832.
5. Lu Z, Li X, Qi Y, Li B, Chen L. Genetic evidence of the causal relationship between chronic liver diseases and musculoskeletal disorders. *J Transl Med*. 2024;22:138.
6. Biswas S, Samanta A. Immune therapies in intermediate-advanced unresectable hepatocellular carcinoma: changing the therapeutic landscape. *World J Gastroenterol*. 2025;31:103267.
7. Sequeira LM, Ozturk NB, Sierra L, Gurakar M, Toruner MD, Zheng M, Simsek C, Gurakar A, Kim AK. Hepatocellular carcinoma and the role of liver transplantation: an update and review. *J Clin Transl Hepatol*. 2025;13:327–38.
8. Ali I, Wani WA, Haque A, Saleem K. Glutamic acid and its derivatives: candidates for rational design of anticancer drugs. *Future Med Chem*. 2013;5:961–78.
9. Ali I, Wani WA, Saleem K, Wesselinova D. Syntheses, DNA binding and anticancer profiles of L-glutamic acid ligand and its copper(II) and ruthenium(III) complexes. *Med Chem*. 2013;9:11–21.
10. Ali I, Wani WA, Khan A, Haque A, Ahmad A, Saleem K, Manzoor N. Synthesis and synergistic antifungal activities of a pyrazoline based ligand and its copper(II) and nickel(II) complexes with conventional antifungals. *Microb Pathog*. 2012;53:66–73.
11. Zhao M, Wang L, Wang M, Zhou S, Lu Y, Cui H, Racanelli AC, Zhang L, Ye T, Ding B, et al. Targeting fibrosis, mechanisms and clinical trials. *Signal Transduct Target Ther*. 2022;7:206.
12. Lappano R, Maggiolini M. G protein-coupled receptors: novel targets for drug discovery in cancer. *Nat Rev Drug Discov*. 2011;10:47–60.
13. Congreve M, de Graaf C, Swain NA, Tate CG. Impact of GPCR structures on drug discovery. *Cell*. 2020;181:81–91.
14. Hilger D, Masureel M, Kobilka BK. Structure and dynamics of GPCR signaling complexes. *Nat Struct Mol Biol*. 2018;25:4–12.
15. Jia Y, Lu W, Xie H, Sheng Y, Wang L, Lv W, Ling L, Dong J, Jia X, Wu S, et al. Upregulation of Siglec-6 induces mitochondrial dysfunction by promoting GPR20 expression in early-onset preeclampsia. *J Transl Med*. 2024;22:674.
16. Zhuang J, Wang Y, Wu X, Peng Z, Huang Z, Zhao C, Shen B. SIGMAR1 screened by a GPCR-related classifier regulates Endoplasmic reticulum stress in bladder cancer. *J Transl Med*. 2025;23:417.
17. Liu M, Parker RM, Darby K, Eyre HJ, Copeland NG, Crawford J, Gilbert DJ, Sutherland GR, Jenkins NA, Herzog H. GPR56, a novel secretin-like human G-protein-coupled receptor gene. *Genomics*. 1999;55:296–305.
18. Luo R, Jeong SJ, Jin Z, Strokes N, Li S, Piao X. G protein-coupled receptor 56 and collagen III, a receptor-ligand pair, regulates cortical development and lamination. *Proc Natl Acad Sci U S A*. 2011;108:12925–30.
19. Xu L, Begum S, Hearn JD, Hynes RO. GPR56, an atypical G protein-coupled receptor, binds tissue transglutaminase, TG2, and inhibits melanoma tumor growth and metastasis. *Proc Natl Acad Sci U S A*. 2006;103:9023–8.
20. Little KD, Hemler ME, Stipp CS. Dynamic regulation of a GPCR-tetraspanin-G protein complex on intact cells: central role of CD81 in facilitating GPR56-Galpha Q/11 association. *Mol Biol Cell*. 2004;15:2375–87.
21. Singh AK, Lin HH. The role of GPR56/ADGRG1 in health and disease. *Biomed J*. 2021;44:534–47.
22. Fan Y, Yan XY, Guan W. GPR56, an adhesion GPCR with multiple roles in human diseases, current status and future perspective. *Curr Drug Targets*; 2024.
23. Ke N, Ma H, Diedrich G, Chionis J, Liu G, Yu DH, Wong-Staal F, Li QX. Biochemical characterization of genetic mutations of GPR56 in patients with bilateral frontoparietal polymicrogyria (BFPP). *Biochem Biophys Res Commun*. 2008;366:314–20.
24. Giera S, Luo R, Ying Y, Ackerman SD, Jeong SJ, Stoveken HM, Folts CJ, Welsh CA, Tall GG, Stevens B et al. Microglial transglutaminase-2 drives Myelination and Myelin repair via GPR56/ADGRG1 in oligodendrocyte precursor cells. *Elife* 2018, 7.
25. Belzeaux R, Gorgievski V, Fiori LM, Lopez JP, Grenier J, Lin R, Nagy C, Ibrahim EC, Gascon E, Courtet P, et al. GPR56/ADGRG1 is associated with response to antidepressant treatment. *Nat Commun*. 2020;11:1635.



26. Ji B, Feng Y, Sun Y, Ji D, Qian W, Zhang Z, Wang Q, Zhang Y, Zhang C, Sun Y. GPR56 promotes proliferation of colorectal cancer cells and enhances metastasis via epithelial-mesenchymal transition through PI3K/AKT signaling activation. *Oncol Rep.* 2018;40:1885–96.
27. Chiang NY, Peng YM, Juang HH, Chen TC, Pan HL, Chang GW, Lin HH. GPR56/ADGRG1 activation promotes melanoma cell migration via NTF dissociation and CTF-Mediated Galpha12/13/RhoA signaling. *J Invest Dermatol.* 2017;137:727–36.
28. Chen T, Shi Z, Zhao Y, Meng X, Zhao S, Zheng L, Han X, Hu Z, Yao Q, Lin H, et al. LncRNA Airn maintains LSEC differentiation to alleviate liver fibrosis via the KLF2-eNOS-sGC pathway. *BMC Med.* 2022;20:335.
29. Zhang K, Shi Z, Zhang M, Dong X, Zheng L, Li G, Han X, Yao Z, Han T, Hong W. Silencing LncRNA Lfar1 alleviates the classical activation and pyroptosis of macrophage in hepatic fibrosis. *Cell Death Dis.* 2020;11:132.
30. Zhang K, Zhang M, Yao Q, Han X, Zhao Y, Zheng L, Li G, Liu Q, Chang Y, Zhang P, et al. The hepatocyte-specifically expressed lnc-HSER alleviates hepatic fibrosis by inhibiting hepatocyte apoptosis and epithelial-mesenchymal transition. *Theranostics.* 2019;9:7566–82.
31. Zhang K, Han Y, Hu Z, Zhang Z, Shao S, Yao Q, Zheng L, Wang J, Han X, Zhang Y, et al. SCARNA10, a nuclear-retained long non-coding RNA, promotes liver fibrosis and serves as a potential biomarker. *Theranostics.* 2019;9:3622–38.
32. Zhang K, Han X, Zhang Z, Zheng L, Hu Z, Yao Q, Cui H, Shu G, Si M, Li C, et al. The liver-enriched lnc-LFAR1 promotes liver fibrosis by activating TGFbeta and Notch pathways. *Nat Commun.* 2017;8:144.
33. Zheng S, Li H, Dong H, Qi F, Zhang B, Yu Q, Lin B, Jiang H, Du H, Liu Y, Yu J. A preliminary study of T-2 toxin that cause liver injury in rats via the NF-kB and NLRP3-mediated pyroptosis pathway. *Toxicon.* 2024;249:108060.
34. Lala T, Hall RA. Adhesion G protein-coupled receptors: structure, signaling, physiology, and pathophysiology. *Physiol Rev.* 2022;102:1587–624.
35. Rosa M, Noel T, Harris M, Ladds G. Emerging roles of adhesion G protein-coupled receptors. *Biochem Soc Trans.* 2021;49:1695–709.
36. Han X, Guo B, Zhao S, Li Y, Zhu J, He Y, Wang J, Yao Q, Shao S, Zheng L, et al. LncRNA Helf promotes hepatic inflammation and fibrosis by interacting with PTBP1 to facilitate PIK3R5 mRNA stabilization. *Cell Mol Biol Lett.* 2023;28:77.
37. Shi Z, Zhang K, Chen T, Zhang Y, Du X, Zhao Y, Shao S, Zheng L, Han T, Hong W. Transcriptional factor ATF3 promotes liver fibrosis via activating hepatic stellate cells. *Cell Death Dis.* 2020;11:1066.
38. Zhang K, Zhang MX, Meng XX, Zhu J, Wang JJ, He YF, Li YH, Zhao SC, Shi ZM, Zheng LN, et al. Targeting GPR65 alleviates hepatic inflammation and fibrosis by suppressing the JNK and NF-kappaB pathways. *Mil Med Res.* 2023;10:56.
39. Guo R, Jia X, Ding Z, Wang G, Jiang M, Li B, Chen S, Xia B, Zhang Q, Liu J, et al. Loss of MLKL ameliorates liver fibrosis by inhibiting hepatocyte necroptosis and hepatic stellate cell activation. *Theranostics.* 2022;12:5220–36.
40. Shao S, Zhang Y, Li G, Yu Z, Cao Y, Zheng L, Zhang K, Han X, Shi Z, Cui H, et al. The dynamics of cell death patterns and regeneration during acute liver injury in mice. *FEBS Open Bio.* 2022;12:1061–74.
41. Wang Y, Gao W, Shi X, Ding J, Liu W, He H, Wang K, Shao F. Chemotherapy drugs induce pyroptosis through caspase-3 cleavage of a gasdermin. *Nature.* 2017;547:99–103.
42. Shi J, Zhao Y, Wang K, Shi X, Wang Y, Huang H, Zhuang Y, Cai T, Wang F, Shao F. Cleavage of GSDMD by inflammatory caspases determines pyroptotic cell death. *Nature.* 2015;526:660–5.
43. Xiao Y, Zhao C, Tai Y, Li B, Lan T, Lai E, Dai W, Guo Y, Gan C, Kostallari E, et al. STING mediates hepatocyte pyroptosis in liver fibrosis by epigenetically activating the NLRP3 inflammasome. *Redox Biol.* 2023;62:102691.
44. Wree A, Eguchi A, McGeough MD, Pena CA, Johnson CD, Canbay A, Hoffman HM, Feldstein AE. NLRP3 inflammasome activation results in hepatocyte pyroptosis, liver inflammation, and fibrosis in mice. *Hepatology.* 2014;59:898–910.
45. Gaul S, Leszczynska A, Alegre F, Kaufmann B, Johnson CD, Adams LA, Wree A, Damm G, Seehofer D, Calvente CJ, et al. Hepatocyte pyroptosis and release of inflammasome particles induce stellate cell activation and liver fibrosis. *J Hepatol.* 2021;74:156–67.
46. Zhang K, Chang Y, Shi Z, Han X, Han Y, Yao Q, Hu Z, Cui H, Zheng L, Han T, Hong W. omega-3 PUFAs ameliorate liver fibrosis and inhibit hepatic stellate cells proliferation and activation by promoting YAP/TAZ degradation. *Sci Rep.* 2016;6:30029.
47. Luedde T, Schwabe RF. NF-kappaB in the liver—linking injury, fibrosis and hepatocellular carcinoma. *Nat Rev Gastroenterol Hepatol.* 2011;8:108–18.
48. Guo Q, Jin Y, Chen X, Ye X, Shen X, Lin M, Zeng C, Zhou T, Zhang J. NF-kappaB in biology and targeted therapy: new insights and translational implications. *Signal Transduct Target Ther.* 2024;9:53.

## Publisher's note

Springer Nature remains neutral with regard to jurisdictional claims in published maps and institutional affiliations.